scientific reports

Check for updates

OPEN

Conserved interactions required for inhibition of the main protease of severe acute respiratory syndrome coronavirus 2 (SARS-CoV-2)

Alina Shitrit[1], Daniel Zaidman[2], Ori Kalid[3], Itai Bloch[4], Dvir Doron[5], Tali Yarnizky[6], Idit Buch[7], Idan Segev[8], Efrat Ben-Zeev[9], Elad Segev[10] & Oren Kobiler[1]✉

The COVID-19 pandemic caused by the SARS-CoV-2 requires a fast development of antiviral drugs. SARS-CoV-2 viral main protease (Mpro, also called 3C-like protease, 3CLpro) is a potential target for drug design. Crystal and co-crystal structures of the SARS-CoV-2 Mpro have been solved, enabling the rational design of inhibitory compounds. In this study we analyzed the available SARS-CoV-2 and the highly similar SARS-CoV-1 crystal structures. We identified within the active site of the Mpro, in addition to the inhibitory ligands' interaction with the catalytic C145, two key H-bond interactions with the conserved H163 and E166 residues. Both H-bond interactions are present in almost all co-crystals and are likely to occur also during the viral polypeptide cleavage process as suggested from docking of the Mpro cleavage recognition sequence. We screened in silico a library of 6900 FDA-approved drugs (ChEMBL) and filtered using these key interactions and selected 29 non-covalent compounds predicted to bind to the protease. Additional screen, using DOCKovalent was carried out on DrugBank library (11,414 experimental and approved drugs) and resulted in 6 covalent compounds. The selected compounds from both screens were tested in vitro by a protease activity inhibition assay. Two compounds showed activity at the 50 µM concentration range. Our analysis and findings can facilitate and focus the development of highly potent inhibitors against SARS-CoV-2 infection.

The raging pandemic caused by SARS-CoV-2 requires a rapid response of the biomedical community[1,2]. However, novel vaccines and antivirals require time for development, thus repurposing of available drugs is a fast alternative and many attempts using different approaches are made[3–6]. Antiviral drugs are traditionally aimed at viral enzymes and are able to cure or reduce symptoms in several viral infections (HIV, HCV and HSV-1[7]).

SARS-CoV-2, the causative agent of COVID-19, belongs to the genus *Betacoronavirus* and is closely related to SARS-CoV-1, the causative agent of the SARS pandemic outbreak in 2003[8]. Coronaviruses are unsegmented single-stranded positive-stranded RNA viruses, featuring the largest known viral RNA genomes (26 to 32 kilobases in length) infecting humans[9].

SARS-CoV-2 genome contains 14 open reading frames (ORFs) encoding 27 proteins. First two ORFs at 5′ untranslated region are coding for overlapping polyproteins (replicase 1a (pp1a) and replicase 1ab (pp1ab)) approximately 450kD and 750kD, respectively. The two polyproteins, pp1a and pp1ab, mediate all the functions required for viral replication and transcription. The longer polyprotein (pp1ab) encodes for 15 nonstructural proteins (viral proteins that are not part of the virions) collectively involved in virus replication and possibly in immune evasion.

[1]The Department of Clinical Microbiology and Immunology, Sackler School of Medicine, Tel-Aviv University, 69978 Tel Aviv, Israel. [2]Department of Organic Chemistry, Weizmann Institute of Science, Rehovot, Israel. [3]Pardes Hana, Israel. [4]Biotechnology Department, Migal - Galilee Research Institute, Kiryat-Shmona, Israel. [5]Chemical & Computational Toxicology, Non-Clinical Development, Global R&D, Teva Pharmaceutical Industries Ltd., Netanya, Israel. [6]Tali Yarnizky Scientific Consulting, Maccabim-Reut, Israel. [7]Emendo Biotherapeutics Ltd., Ness Ziona, Israel. [8]Rishon-LeZion, Israel. [9]The Nancy and Stephen Grand Israel National Center for Personalized Medicine, Weizmann Institute of Science, Rehovot, Israel. [10]Department of Applied Mathematics, Faculty of Science, Holon Institute of Technology, Holon, Israel. ✉email: okobiler@tauex.tau.ac.il

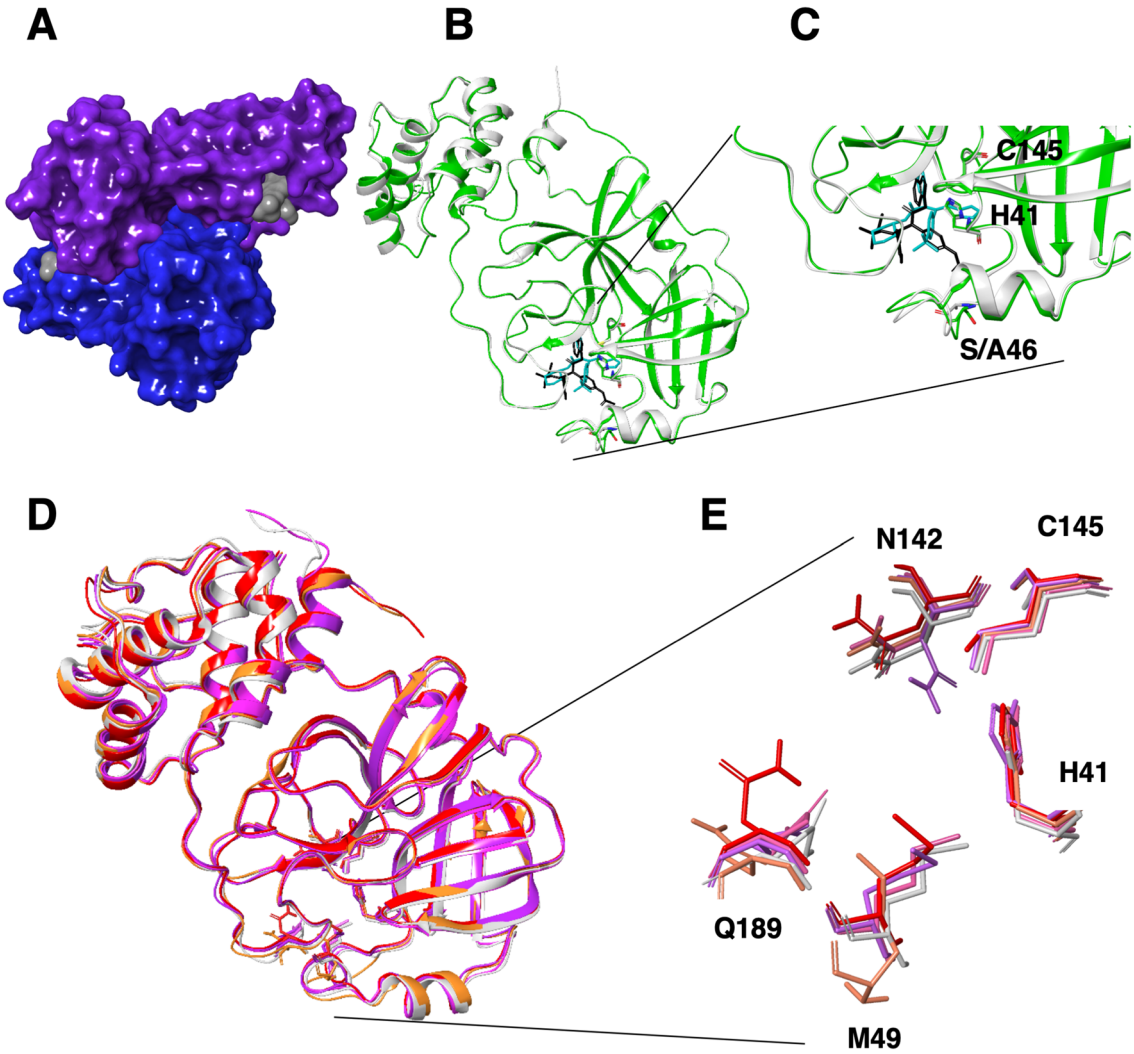

Figure 1. Structural overview of main protease homodimer of SARS-CoV-2 and its binding site. (**A**) Surface topology of SARS-CoV-2 Mpro homodimer in complex with the covalent α-ketoamide inhibitor (PDB structure 6Y2F). The two monomers are colored in blue and purple and the inhibitors are represented in gray. (**B**) Superimposition of SARS-CoV-2 Mpro (6W63, shown as ribbon and colored in green) and SARS-CoV-1 (4MDS, shown as ribbon and colored in gray) in complex with their non-covalent inhibitors X77 (shown as sticks and colored in cyan) and ML300 (shown as sticks and colored in black), respectively, shown as ribbons. The catalytic residues H41 and C145 are in sticks. The different amino acids SARS-CoV-2 S46 and CoV-1 A46 are shown in sticks. (**C**) Magnified view of (**B**) (binding site) (**D**) Superimposition of the most diverse structures of SARS-CoV-2 and SARS-CoV-1 (available at that time) are shown in ribbons. SARS-CoV-1, 2ZU5 (gray), SFfARS-CoV-2, 5R80 (purple), SARS-CoV-2, 6LU7 (pink), SARS-CoV-2, 6M03 (red), SARS-CoV-2, 6Y2F (orange). Residues within this site Q189, M49 and N142 and the catalytic residues H41 and C145 are represented in sticks. (**E**) Magnified view of (**D**). All images were drawn using the maestro software (https://www.schrodinger.com/maestro).

The functional polypeptides are released from the polyproteins by extensive proteolytic processing. This is primarily achieved by the main protease (Mpro), along with the papain-like protease. Together, they cleave the amino acid backbone at 11 sites on the large polyprotein. This cleavage site involves Leu-Gln↓(Ser/Ala/Gly) sequences (the cleavage site is indicated by ↓)[10]. This cleavage pattern appears to be conserved in the Mpro of SARS-CoV-1.

The Mpro of the coronaviruses is a homodimer. It cleaves the polyprotein using its catalytic dyad that contains the catalytic residues Histidine 41 (H41) and Cysteine 145 (C145) (Fig. 1A–C). All of the residues within the active site, including the catalytic residues and adjacent binding residues (polypeptide binding site) belong to one monomer, except for one (Serine 1) from the second monomer[11].

Several co-crystal structures of the SARS-CoV-2 Mpro were recently solved, enabling the rational design of specific inhibitory compounds[12–15]. The binding site of all the ligands from the co-crystals is found within the Mpro active site. The close relationship of SARS-CoV-2 to SARS-CoV-1 is reflected by high sequence identity of 96.1% and similarity of 99% among their entire proteases protein sequence[16]. In the vicinity of the binding site, the only residue that differs is positioned at residue 46. In SARS-CoV-2 it is a Serine and in SARS-CoV-1 it is an

Alanine; however, their side chains point out of the binding site (Fig. 1C). Moreover, a recent study showed that the two binding sites have similar substrate specificities[17].

The high similarity between the two viruses' proteins and the fact that their active sites are practically identical, enable the use of SARS-CoV-1 co-crystals[18–35] in addition to the available SARS-CoV-2 co-crystals, for understanding the vicinity of the binding site region and defining the important interactions within the SARS-CoV-2 binding site with its inhibitors. In this regard, it was suggested that drugs developed against SARS-CoV-1 might be effective to treat SARS-CoV-2[16]. However, these compounds remained in the preclinical or early clinical stage, without further development into an approved medicine.

In this study, we analyzed the available SARS-CoV-1 and SARS-CoV-2 Mpro co-crystal structures and the developed SARS-CoV-1 inhibitory compounds and identified key interactions required to identify and develop an active inhibitor for the main protease. We conducted a virtual screen using a library of only FDA-approved drugs against SARS-CoV-2 Mpro structure from protein data bank (PDB) [6W63][13] using three docking software tools (GOLD[36] and Glide[37–39] and DOCKovalent[40]). Several compounds were selected and tested in vitro using a protease inhibition assay.

Results

Analysis of co-crystals flexibility. To identify the flexibility of the Mpro binding site, we superimposed the SARS-CoV-1 and SARS-CoV-2 apo and co-crystal structures available at the time of our study in the PDB (Table 1). We selected the five most distinct, root-mean-square deviation (RMSD)-wise, structures within the 3D space of the binding site. The selected structures were 2ZU5, 5R80, 6LU7, 6M03, 6Y2F. Three flexible residues within the binding site showed variation in their positions between the different structures: Glutamine 189, Methionine 49 and Asparagine 142 (Fig. 1D,E).

Covalent and non-covalent co-crystal interactions. To find the essential interactions required for inhibition of the SARS-CoV-2 Mpro, we analyzed the interactions observed with both covalent and non-covalent inhibitors (Table 1). Most of the co-crystals for SARS-CoV-1 and SARS-CoV-2 contain covalent inhibitors (32 structures). To date, only 6 co-crystals contain non-covalent inhibitors.

Analyzing the co-crystal interactions of the non-covalent inhibitors revealed that the two SARS-CoV-2 co-crystallized ligands, X77 [6W63] and N3 [6M2N], form H-bonds with protein NH donors: Histidine 163 (H163) and Glutamic acid 166 (E166) backbone. Interestingly, 3WL mediates the H-bond interaction with H163 through a water molecule (Fig. 2A). In SARS-CoV-1 co-crystals, three out of the four structures showed both H163 and E166 backbone interactions and all exhibited the E166 backbone H-bond interaction. Interestingly, F3F [2GZ8] mediates the E166 backbone interaction through a water molecule.

Additional interactions were observed with the following amino acids: The catalytic H41 with D3F [2GZ7] and ML300 [4MDS]. The catalytic C145 forms a H-bond with F3F [2GZ8]. G143 backbone with X77 [6W63] and N142 and F140 with F3F [2GZ8]. Many hydrophilic moieties of the ligands are surrounded by water molecules that mediate the interaction of the inhibitor with the protein.

All covalent compounds interact with the catalytic C145 in the co-crystals. Interestingly, most (31 out of 32) comprise also a non-covalent interaction, H-bond with H163 similarly to the non-covalent compounds. All of the covalent and non-covalent inhibitors present a H-bond acceptor to the side chain imidazole ring of H163 (see for example Fig. 2A–C). The only exception, presenting a H-bond donor towards H163, is SLH inhibitor [5C5N[(Fig. 2D). Since the hydrogen can reside on either nitrogen, (N1-H or N3-H tautomers) it interacts with the imidazole N acceptor.

E166 backbone that is interacting with all non-covalent ligands is also a key residue for most covalent ligands. Most ligands (30 out of 32) form H-bond interactions with the E166 backbone NH and some form an additional interaction with the E166 backbone carbonyl oxygen (for example, α-ketoamide 13b [6Y2F], ZU3 [2ZU4], N3 [2AMQ and 6LU7] and ZU5 [2ZU5], Fig. 2B,C). Few structures mediate E166 backbone interaction through a water molecule (for example, F3F [4TWY] and SDJ [5C5O]) (Table 1). In addition to E166 backbone interactions, some ligands interact with E166 side chain either via salt bridge (for example, N3 [6LU7] and SLH [5C5N]) or through a H-bond interaction (for example, α-ketoamide 13b [6Y2F] and ZU3 [2ZU4], Fig. 2B,C).

Other backbone interactions can be detected with G143 [6LU7, 6Y2F and 2ZU4], H164 [6LU7] and F140 [2GX4 and 6LU7]. In addition, a side chain interaction is formed by ZU3 [2ZU4] with the flexible residue Q189 (Figs. 2B,C).

Docking of the cleavage recognition sequence. The proteolytic activity of Mpro catalyzes cleavage between Glutamine and Serine within the viral polypeptides. To characterize the interactions required for cleavage, we analyzed two co-crystals with peptidomimetic inhibitors [2A5I, 3VB5]. In these structures, the side chain of the catalytic C145 binds the peptide Serine backbone. The catalytic C145 side chain is rigid in all co-crystals except for [2A5I] in which the side chain adopts a unique conformation. Interestingly, the peptide Glutamine side chain of the cleavage site is anchored by a H-bond interaction with the H163 imidazole (Fig. 2E).

To characterize the interactions of the cleavage recognition sequence peptide we chose, based on the peptidomimetic inhibitors, the following sequence: Ala, Val, Leu, Gln, Ser, Ala, Gly. We docked (using Glide) the recognition sequence peptide to SARS CoV-2 6LU7 crystal structure and superimposed the two co-crystals with the peptides [2A5I, 3VB5]. The Glutamine within the recognition sequence adopted the same conformation as in the two co-crystals, presenting the same H-bond interaction with H163 imidazole (Fig. 2F). In addition, the peptide's Valine and Alanine backbone interact with the E166 backbone (through water molecules).

Virus	Binding type	Release date	Resolution	Ligand	Activity	PDB ID	H163	E166bb	Ref
SARS-CoV-2	Non-covalent	03/2020	2.1 Å	X77		6W63	Yes	Yes	13
SARS-CoV-2	Non-covalent	04/2020	1.56 Å	3WL		6M2N	Yes*	Yes	14
SARS-CoV-2	Covalent	03/2020	1.95 Å	α-ketoamide 13b	IC50 = 0.67 μM	6Y2F	Yes	Yes	15
SARS-CoV-2	Covalent	03/2020	2.2 Å	α-ketoamide 13b	IC50 = 0.67 μM	6Y2G	Yes	Yes	15
SARS-CoV-2	Covalent	02/2020	2.16 Å	N3		6LU7	Yes	Yes	12
SARS-CoV-1	Non-covalent	02/2013	1.6 Å	ML300/23H	IC50 = 6.2 μM	4MDS	Yes	Yes	30
SARS-CoV-1	Non-covalent	08/2006	1.86 Å	D3F	IC50 = 0.3 μM	2GZ7	No	Yes	27
SARS-CoV-1	Non-covalent	08/2006	1.97 Å	F3F	IC50 = 3 μM	2GZ8	No	Yes*	27
SARS-CoV-1	Non-covalent	07/2007	1.80 Å	WR1	Ki = 2.2 μM	2OP9	No	Yes	21
SARS-CoV-1	Non-covalent	01/2013	1.96 Å	0EN	IC50 = 4.8 μM	3V3M	Yes	Yes	22
SARS-CoV-1	Covalent	03/2020	1.9 Å	OEW		6Y7M	Yes	Yes	33
SARS-CoV-1	Covalent	06/2016	1.69 Å	SLH		5C5N	Yes**	Yes	28
SARS-CoV-1	Covalent	06/2016	1.59 Å	SDJ		5C5O	Yes	Yes*	28
SARS-CoV-1	Covalent	12/2012	1.95 Å	C4Z		3VB5	Yes	Yes	18
SARS-CoV-1	Covalent	12/2012	2.5 Å	C6Z		3VB6	Yes	Yes	18
SARS-CoV-1	Covalent	01/2009	1.65 Å	TG-0205486/ZU5	Ki = 0.099 μM	2ZU5	Yes	Yes	23
SARS-CoV-1	Covalent	01/2009	1.93 Å	TG-0204998/ZU3	Ki = 0.038 μM	2ZU4	Yes	Yes	23
SARS-CoV-1	Covalent	09/2005	1.85 Å	N9	Ki = 6.7 μM	2AMD	Yes	Yes	31
SARS-CoV-1	Covalent	09/2005	2.3 Å	N3		2AMQ	Yes	Yes	31
SARS-CoV-1	Covalent	05/2006	1.93 Å	NOL	Ki = 0.053 μM	2GX4	Yes	Yes	32
SARS-CoV-1	Covalent	10/2005	1.88 Å	aza-peptide epoxide	Ki = 18 μM	2A5I	Yes	Yes	24
SARS-CoV-1	Covalent	08/2005	2.0 Å	N1	Ki = 10.7 μM	1WOF	Yes	Yes	31
SARS-CoV-1	Covalent	10/2005	2.3 Å	AZP	Ki = 18 μM	2A5K	Yes	Yes	24
SARS-CoV-1	Covalent	08/2006	1.9 Å	CY6	IC50 = 70 μM	2ALV	Yes	Yes	20
SARS-CoV-1	Covalent	02/2008	1.9 Å	CYV	IC50 = 80 μM	2QIQ	Yes	Yes	19
SARS-CoV-1	Covalent	12/2006	2.0 Å	AZP		2GTB	Yes	Yes	25
SARS-CoV-1	Covalent	09/2011	1.99 Å	S89	Ki = 2.24 μM	3SN8	No	Yes	35
SARS-CoV-1	Covalent	09/2011	1.89 Å	PRD_000 772	Ki = 8.27 μM	3SND	Yes	No	35
SARS-CoV-1	Covalent	07/2012	1.69 Å	G75		3SZN	Yes	Yes	34
SARS-CoV-1	Covalent	08/2012	1.99 Å	G81		3TIT	Yes	Yes	34
SARS-CoV-1	Covalent	08/2012	2.08 Å	G82		3TIU	Yes	Yes	34
SARS-CoV-1	Covalent	09/2012	1.99 Å	G83		3TNS	Yes	Yes	34
SARS-CoV-1	Covalent	09/2012	1.59 Å	G85		3TNT	Yes	Yes	34
SARS-CoV-1	Covalent	02/2015	2.42 Å	3A7	IC50 = 63 μM	4TWW	Yes	Th	29
SARS-CoV-1	Covalent	02/2015	1.6 Å	3BL	IC50 = 108 μM	4TWY	Yes	Yes*	29
SARS-CoV-1	Covalent	02/2015	1.89 Å	3X5	IC50 = 240 μM	4WY3	Yes	No	29
SARS-CoV-1	Covalent	03/2018	2.0 Å	8O5		5N5O	Yes	Yes	26
SARS-CoV-1	Covalent	02/2018	1.62 Å	D03		5N19	Yes	Yes	26

Table 1. SARS-CoV-1/2 Mpro covalent and non-covalent co-crystals PDB structures. A list of all PDB structures used in this work and their interactions with the two key residues H163 and E166 backbone (bb) are summarized. The known activity from the literature is mentioned when available in either inhibition concentration of 50% (IC50) or inhibitory constant (Ki). *-represent interaction through water molecule. **-introduces a donor to the imidazole. th-Theoretically represent interaction through water molecule, although the water molecule is not present in the structure.

Docking of controls: known SARS-CoV-1 Mpro inhibitors. Since the SARS-CoV-1 outbreak in 2003, several studies have developed inhibitors for Mpro of SARS-Cov-1[22,23,27,31,32,41]. To verify that our observed interactions are required for Mpro inhibition, we docked non-covalent SARS-CoV-1 Mpro inhibitors to the SARS-CoV-2 Mpro binding site [6W63]. The same two common interactions (H163 and E166) were present in all compounds tested (see for example few known inhibitors in Fig. 3).

In summary, the two hydrophilic interactions with H163 and E166 backbone exist in most of the covalent and non-covalent co-crystal ligands and all of these co-crystals show at least one of these interactions. The known inhibitors show the same pattern of interactions and these interactions seem to play a role in the recognition sequence binding, thus highlighting them as biologically significant. Therefore, in the screening process these interactions were chosen as filtering criteria, allowing to pass only poses that satisfied at least one of these two interactions, for further analysis.

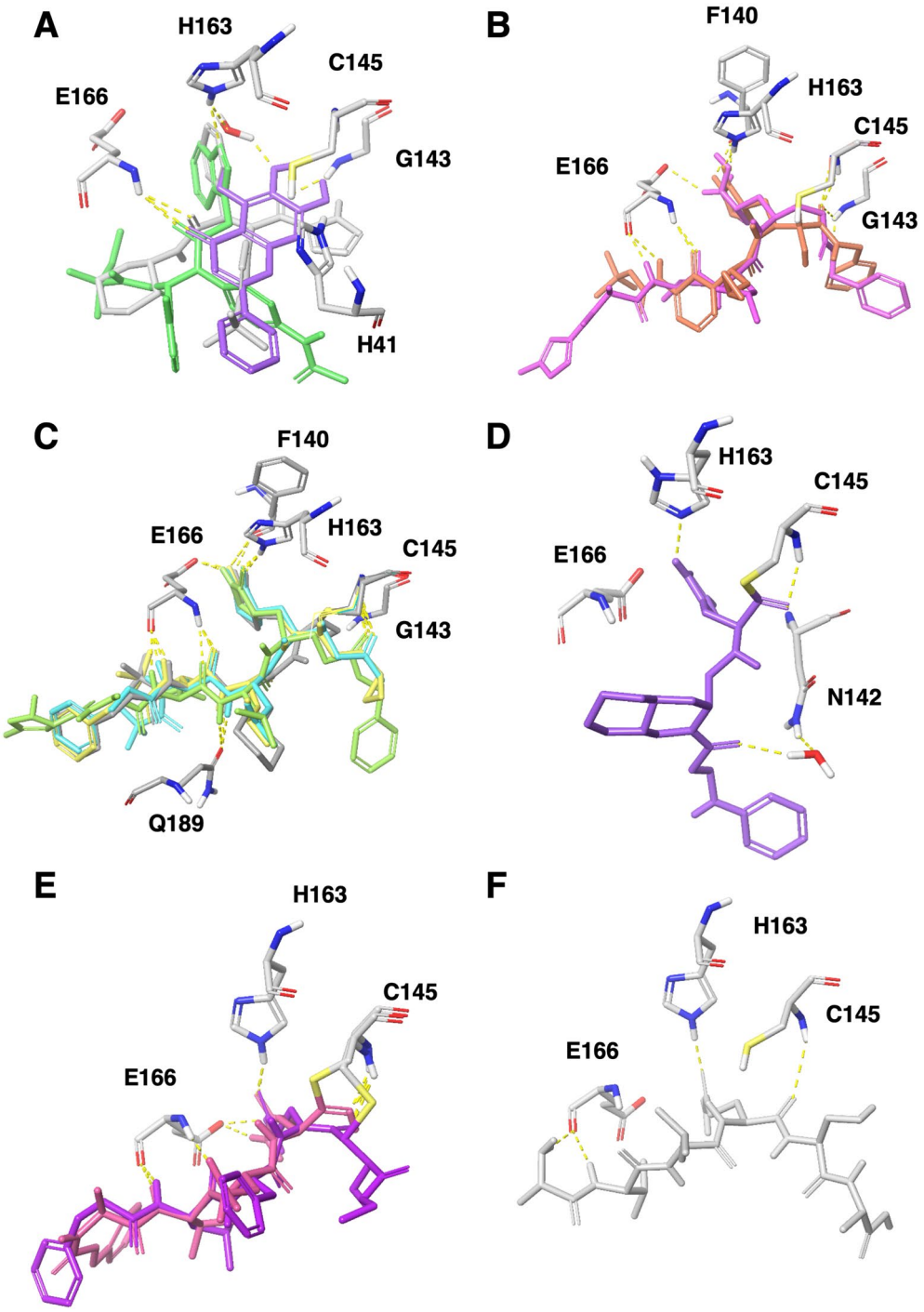

Figure 2. Co-crystals interactions and important residues. (**A**) Superimposition of non-covalent co-crystals 6W63 (gray), 4MDS (green) and 6M2N (purple) with protein residues shown in sticks (colored by element). (**B**) Superimposition of covalent co-crystals 6LU7 (pink), 6Y2F (orange). (**C**) Superimposition of covalent co-crystals 2GX4 (gray), 2ZU4 (cyan), 2AMQ (green), 2ZU5 (yellow), shown in sticks. (**D**) 5C5N (purple), shown in sticks. Protein interactions residues are shown in sticks. (**E**) Two co-crystals with peptides 2A5I (purple), 3VB5 (pink). (**F**) The recognition sequence peptide docked within the 6LU7 (gray). All images were drawn using the maestro software (https://www.schrodinger.com/maestro).

In addition, the Schrödinger SiteMap tool[42,43] identified two hydrophobic regions within the vicinity of the binding site and we found that most of the covalent and non-covalent co-crystal ligands and the known inhibitors introduced hydrophobic moieties within those regions.

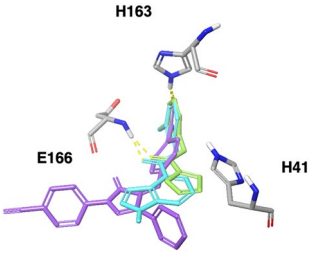

Figure 3. SARS-CoV-1 developed inhibitor docked to Mpro 6W63 PDB structure. Zhang2007 cmp37 (green), ghosh2008 cmp10 (cyan), Lu2006_Pyrazolone cmpd2p (purple). Important residues for interactions are shown in sticks. Image was drawn using the maestro software (https://www.schrodinger.com/maestro).

Non-covalent docking using GOLD and Glide. To identify possible inhibitors from the FDA-approved drugs we used [6W63] protein structure as a template for virtual screening, applying two docking software (as recommended[44]). The prepared ligand set originating from the ChEMBL drug database was docked either using GOLD, outputting 10 conformations (poses) for each compound resulting in 46,190 poses (3634 unique drugs), or using Glide, outputting at most 5 conformations (poses) per compound resulting in 22,004 poses (3620 unique drugs).

We filtered the poses based on the two significant interactions identified in our analysis: H163 imidazole H-bond and E166 backbone amine H-bond (see the "Materials and Methods" section for details). We chose the best docking poses that satisfied either one or both of these interactions, resulting in at most three poses for each compound. This stage resulted in 2993 unique compounds poses in GOLD and 1969 unique compounds in Glide. We manually selected the filtered poses resulting in 21 compounds in GOLD and 13 in Glide. Altogether, a total of 29 unique compounds (4 of which were selected in both methods) were selected and sent for assessment using the protease inhibition assay. One compound, selected by the GOLD software, GSK-256066, showed 37% inhibition at concentration of 50 μM (Supplementary Table 1).

Covalent docking using DOCKovalent. Several covalent docking software were developed at Nir London's lab at the Weizmann institute[40]. As there are very few possible known drugs that can perform covalent binding, we used preclinical and clinical compounds from the DrugBank database[45]. This database was filtered to contain only compounds with covalent warheads that can be docked using DOCKovalent (see "Materials and Methods") to: [6M03, 5R7Y, 5R7Z, 6Y2F, 6W63, 4MDS, 2GX4, 6LU7] PDB structures. These compounds were visually inspected and we selected the ones that showed additional interactions to the C145 covalent interaction. We tested 5 nitriles and one Michael acceptor and two of the nitriles (bicalutamide and ruxolitinib) showed 36% and 20% inhibition at 50 μM, respectively (Supplementary Table 2).

Discussion

Antiviral drugs targeting the Mpro of SARS-CoV-2 could support the fight against the global COVID-19 pandemic. Here, to identify possible inhibitors of the SARS-CoV-2 Mpro, we have explored the co-crystal structures of the Mpro proteins of SARS-CoV-2 and SARS-CoV-1. We identified two common interactions involving H163 and E166 that appeared in most co-crystals. We screened in silico drug databases for covalent and non-covalent compounds. Possible compounds were further tested in a protease inhibition assay and we found several compounds that reduce protease activity by more than 30%.

The Mpro protein sequence of SARS-CoV-2 is highly similar (99%) to SARS-CoV-1. In the region of the binding site only one residue is different. Some studies suggested that the differences between the two proteins affected the ability to bind inhibitors[46,47]. On the other hand, several studies and our protease inhibition assay show that inhibitors identified for SARS-CoV-1 Mpro also inhibit SARS-CoV-2 Mpro (see Supplementary Table 3). Further co-crystals of SARS-CoV-1 [2MAQ] and SARS-CoV-2 [6LU7] Mpro with the identical inhibitor (N3) show similar interactions with the protease binding site[12]. Thus, we inferred that the binding to the binding site of both viruses is comparable and therefore we were able to analyze the key interactions based on co-crystals obtained from both viruses.

We identified that all co-crystals have at least one of two key interactions with H163 and E166. Docking of the recognition sequence peptide into the binding site revealed that H163 and E166 form H-bonds with the peptide. Specifically, the imidazole ring of H163 interacts with the conserved Glutamine of the cleavage site[11] while E166 interacts with the Alanine and Valine from the recognition sequence. Interestingly, E166 side chain interacts with Serine 1 NH_2-terminal of the second monomer[11,48]. This salt bridge interaction minimizes the conformational flexibility of E166 backbone and assists in generating the correct orientation of the substrate binding site, which explains the importance of dimerization for the catalytic activity[48]. H163 and E166 amino acids are conserved among all human coronaviruses (2 alpha- and 5 beta-coronaviruses Fig. 4), unlike H164 and Q189 that were previously identified as important interactions of several inhibitors[12,23]. Thus, drugs developed to interact with these amino acids may be effective against all human coronaviruses and could potentially prevent the emergence of viral resistance.

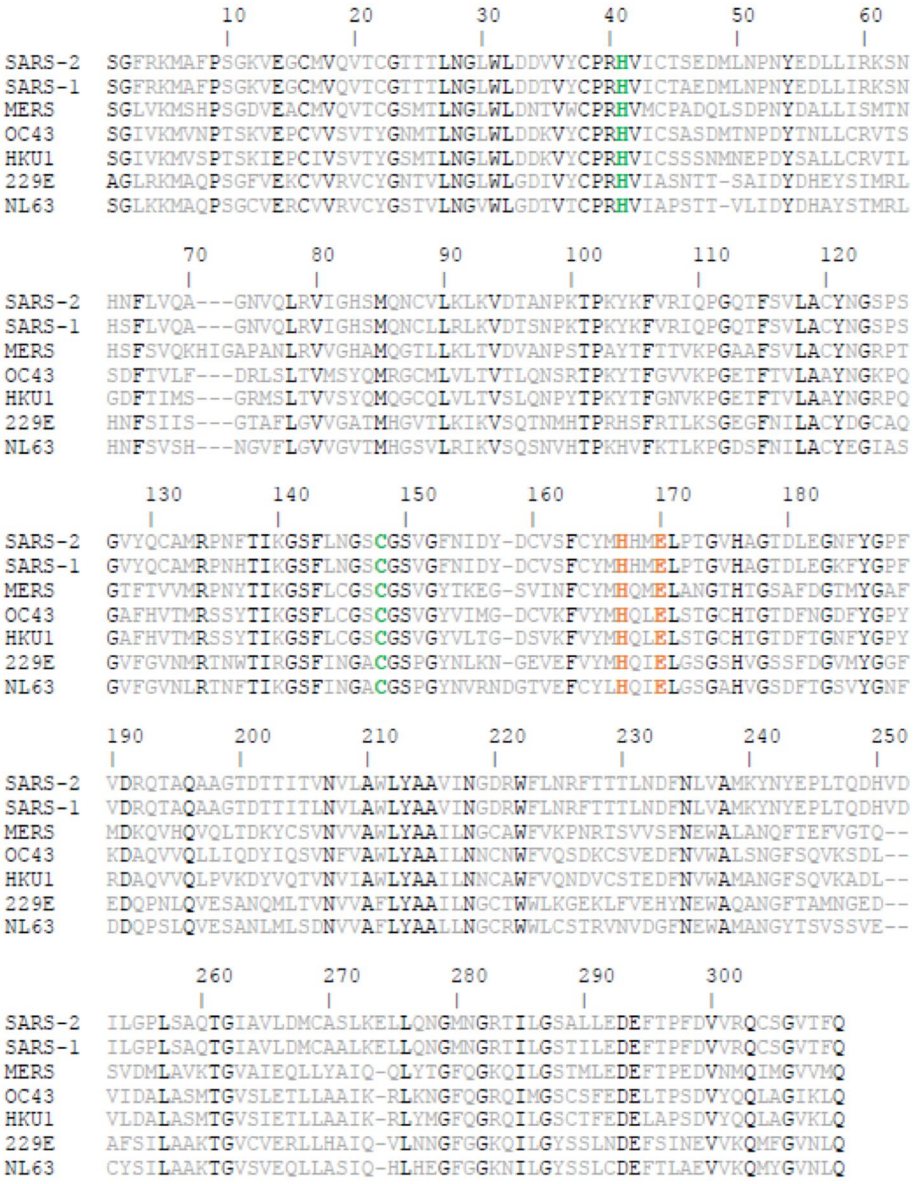

Figure 4. Conservation of human coronaviruses Mpro. Conserved residues are colored in black. Specifically, catalytic dyad residues (H41 and C145) are colored in green. H163 and E166 are colored in orange.

Recent studies have identified several drugs as candidates for Mpro inhibition. Jin et al[12] found 7 inhibitors in their in-vitro high throughput screening. In our analysis, four out of the seven were filtered before docking (below phase 2, and non-FDA medicine). Tideglusib, Disulfiram showed docking poses with E166 in GOLD.

Riva et al[5] found 100 clinical compounds that were found to reduce viral replication by at least 40%. Most of these compounds are preclinical and below phase 2 thus were not included in our focused screen; only seven compounds passed our filtering criteria. In our in-silico screening process, Beclabuvir did not pass the docking. The other six compounds (Chloroquine, Tamibarotene, Mardepodect, Tretinoin, Apilimod, JNJ-42165279) were shown to interact with H163, E166 or both. These compounds further support the importance of the H163, E166 interactions for inhibition of SARS-CoV-2 Mpro.

In addition, several attempts to identify in-silico inhibitors of SARS-CoV-2 Mpro have been already published[49–53]. All of these did not validate their virtual screen results by in-vitro experiments. Further, these studies used either [6LU7] or [6Y2F], as their template for the computational screening. We used [6W63] as the protein structure for our non-covalent docking, as [6W63] ligand is non-covalent while [6LU7] and [6Y2F] ligands are covalent. The protein structure of [6W63] differs from [6LU7] and [6Y2F] in the identified co-crystals flexibility residues M49, Q189 and N142 (Fig. 1D,E). For the covalent docking we used seven different crystal structures (see results) to allow more flexibility in the binding site.

Our two screening analyses resulted in two clinically approved drugs that inhibit the Mpro by over 30% in 50 μM: The first one is GSK-256066, a phosphodiesterase (PDE) 4 inhibitor[54] that was under development in phase 2 for the treatment of chronic obstructive pulmonary disease (COPD), asthma and seasonal allergic

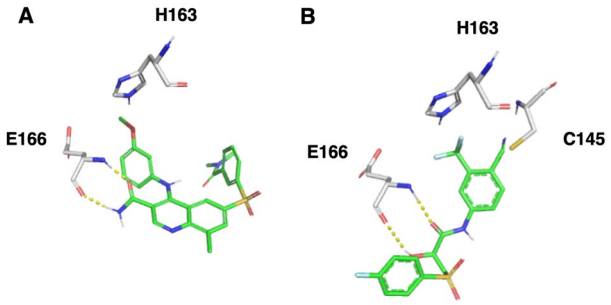

Figure 5. FDA-approved drugs that inhibit Mpro. (**A**) GSK-256066 (colored by element) (**B**) Bicalutamide (colored by element). Important residues for interactions are shown in gray element sticks. All images were drawn using the pymol software (https://pymol.org/2/).

rhinitis. It is administered as an inhalation formulation (powder) and as an intranasal formulation (nasal spray suspension). Our model suggests that GSK-256066 forms a H-bond with H163 and additional two H-bonds with the amine and carbonyl of E166 backbone (Fig. 5). It inhibits the Mpro by 37% at a concentration of 50 μM.

Another drug that showed inhibition of the Mpro is bicalutamide, which was selected from the covalent screening. It contains an aryl nitrile that can covalently bind to the protein. Bicalutamide is an oral non-steroidal anti-androgen for prostate cancer. It is comprised of a 50:50 racemic mixture of the (*R*)- and (*S*)-enantiomers. Bicalutamide binds to the androgen receptor. Our model suggests that its nitrile group covalently binds to C145 and forms two H-bonds with the amine and carbonyl of the E166 backbone (Fig. 5). Bicalutamide was tested in two experiments and inhibited Mpro by 37% and 33% at a concentration of 50 μM.

Several compounds that were previously identified as inhibitors with sub-micromolar potency were active in our protease inhibition assay (Supplementary Table 3). Two of these inhibitors with known sub-micromolar activity, showed limited inhibition (39% and 9%) at a concentration of 50 μM in our protease activity assay (Supplementary Table 3). Thus, GSK-256066 and bicalutamide, that were identified in our protease inhibition assay, have a similar inhibitory activity at the same concentration. These results suggest that more assays should be conducted to test repurposing of these drugs as anti-SARS therapeutics.

In conclusion, our analysis of the structural constraints required for the inhibition of SARS-CoV-2 Mpro has suggested key interactions with several amino acids in the active pocket of the protein. We were able to identify several approved drugs with a potential to inhibit Mpro activity; however, the observed inhibition in our experimental assay suggest that these compounds need to be chemically modified to be considered as potential treatment. In addition, our analysis could be used for further virtual screenings of larger compound databases or for rational drug development.

Materials and methods

Protein data bank (PDB) search. The protein data bank was searched for SARS-CoV/SARS-CoV-1/SARS-CoV-2 Mpro. Non SARS-CoV structures and non-human SARS-CoV like structures were omitted. Co-crystals binding fragments were not added to this analysis due to their non-drug like structures. We anticipate that few of the available structures might be overlooked using these search criteria. All PDB structures found and analyzed are mentioned in Table 1. Throughout the text, PDB IDs are marked with square brackets.

Preparing a drug library from ChEMBL for non-covalent docking. The ChEMBL database contains 6900 drugs in various stages of clinical trials. To focus our computational screen, the following filters were applied: small molecules at clinical phase 2 or higher clinical trials, number of rotatable bonds < 14, Molecular Weight (MW) freebase ranging from 200 to 990, Anatomical Therapeutic Chemical (ATC) Classifications Level1 Description: all groups except D- Dermatologicals and V- Various. This filtering resulted in a 4239-compound library. To prepare the ligands for docking simulations, LigPrep (Schrödinger Release 2020-1: LigPrep, Schrödinger, LLC, New York, NY, 2020) was applied on the exported library. The following settings were used: (a) The OPLS3e force field was chosen[55]; (b) Possible protonation states were generated using Ionizer at a target pH of 7.4 ; (c) All ligands were desalted; (d) No tautomers were generated; (e) At most two stereoisomeric forms were produced per ligand for unspecified chiral centers. These constraints enabled us to expand the initial 4239-compound library to only 4623 ligands.

Preparing a drug library from DrugBank for covalent docking. We used the DrugBank database[45] that includes 11,414 preclinical and clinical small molecules. These compounds were filtered by ≤ 500D MW and ≤ 5 rotatable bonds. Only compounds that contain covalent warheads (Michael acceptors: O = CC = [C;H1,H2] or nitriles) were selected as they can covalently bind the thiol of C145. The filtering resulted in a library of 437 ligands (258 Michael acceptors and 179 nitriles).

Docking. The 4623 prepared ligands originating from ChEMBL were docked using Glide (Schrödinger Release 2020-1: Glide, Schrödinger, LLC, New York, NY, 2020) to the Mpro structure from [6W63], keeping

the protein structure rigid and ligands flexible, with no constraints applied on specific receptor-ligand hydrogen bond (H-bond) interactions. The standard precision (SP) mode of Glide was used based on the OPLS3e force field, writing out at most 5 poses per ligand. The 22,003 conformations (poses) were filtered by requiring at least one of the two key H-bond interactions with H163 and E166. The default maximum H-bond distance criterion of 2.5 Å was stretched to 3.0 Å. This filter resulted in three groups of poses: (a) 517 poses interacting with both H163 and E166; (b) 2088 poses forming a H-bond with H163 only; and (c) 2678 poses forming a H-bond with E166 only. In each of the filtered groups, the pose with the best Glide score per each ligand was selected, resulting in 293, 879 and 1347 poses, respectively. We further narrowed down the number of poses by eliminating drugs with molecular charge below −1 using Maestro's Ligand Filtering utility. Applying this filter resulted in 260, 820 and 1283 poses, respectively. Removing the duplicate poses (i.e. those overlapping with one associated with either or both of the two other groups) resulted in a total of 1969 unique poses.

The 4239 ChEMBL-derived ("pre-Ligprep") drugs were also docked using GOLD Standard docking[36] to Mpro structure from [6W63] resulting in 46,190 poses (10 poses per ligand). Identical filters as in Glide docking were applied resulting in a total of 2993 unique poses that were grouped by interactions to (a) 86 poses interacting with both H163 and E166; (b) 1011 poses forming H-bond with H163 only; and (c) 1896 poses forming H-bond with E166 only.

Selection. In our manual selection we preferred ligands that in addition to one or two important interactions (H163 and E166) also formed interactions with additional residues that were found in the co-crystal structure (for example Gly143 backbone). In addition, we favored compounds that did not violate the two hydrophobic regions within the binding site as calculated by Maestro's SiteMap tool (Schrödinger Release 2020-1: SiteMap, Schrödinger, LLC, New York, NY, 2020[42,43]).

Protease inhibitor activity assay. 35 compounds were obtained as detailed in Supplementary Table 1 and 2. The compounds were prepared in assay ready plates (Greiner 784900) using Labcyte Echo 555 and diluted in DMSO to concentration of 0.5%. 5 nM Mpro and 375 nM [5-FAM]-AVLQSGFR-[Lys(Dabcyl)-K-amide substrate (in 20 mM HEPES pH = 7.3, 50 mM NaCl, 10% Glycerol, 0.01% Tween-20, 1 mM TCEP) were added to the compounds and incubated for 30 min at room temperature. Fluorescence was read at 480/520 ex/em in BMG Pherastar FS.

The Mpro inhibition assay[56] was carried out in the Mantoux Bioinformatics institute of the Nancy and Stephen Grand Israel National Center for Personalized Medicine (INCPM), Weizmann Institute of Science (as part of the COVID Moonshot initiative https://covid.postera.ai/covid/activity_data).

Received: 2 September 2020; Accepted: 17 November 2020
Published online: 30 November 2020

References

1. Sohrabi, C. *et al.* World Health Organization declares global emergency: a review of the 2019 novel coronavirus (COVID-19). *Int. J. Surg.* **76**, 71–76. https://doi.org/10.1016/j.ijsu.2020.02.034 (2020).
2. Wang, C., Horby, P. W., Hayden, F. G. & Gao, G. F. A novel coronavirus outbreak of global health concern. *Lancet* **395**, 470–473. https://doi.org/10.1016/S0140-6736(20)30185-9 (2020).
3. Weston, S. *et al.* Broad anti-coronaviral activity of FDA approved drugs against SARS-CoV-2 in vitro and SARS-CoV in vivo. *bioRxiv*, 2020.2003.2025.008482, https://doi.org/10.1101/2020.03.25.008482 (2020).
4. Saul, S. & Einav, S. Old drugs for a new virus: repurposed approaches for combating COVID-19. *ACS Infect. Dis.* https://doi.org/10.1021/acsinfecdis.0c00343 (2020).
5. Riva, L. *et al.* Discovery of SARS-CoV-2 antiviral drugs through large-scale compound repurposing. *Nature* https://doi.org/10.1038/s41586-020-2577-1 (2020).
6. Panda, P. K. *et al.* Structure-based drug designing and immunoinformatics approach for SARS-CoV-2. *Sci. Adv.* **6**, eabb8097. https://doi.org/10.1126/sciadv.abb8097 (2020).
7. Muller, B. & Krausslich, H. G. Antiviral strategies. *Handb. Exp. Pharmacol.* https://doi.org/10.1007/978-3-540-79086-0_1 (2009).
8. Chan, J. F. *et al.* Genomic characterization of the 2019 novel human-pathogenic coronavirus isolated from a patient with atypical pneumonia after visiting Wuhan. *Emerg. Microbes Infect.* **9**, 221–236. https://doi.org/10.1080/22221751.2020.1719902 (2020).
9. Howley, P. M. & Knipe, D. M. *Fields Virology - Emerging Viruses*. (Lippincott Williams & Wilkins, 2020).
10. Ziebuhr, J., Snijder, E. J. & Gorbalenya, A. E. Virus-encoded proteinases and proteolytic processing in the Nidovirales. *J. Gen. Virol.* **81**, 853–879. https://doi.org/10.1099/0022-1317-81-4-853 (2000).
11. Yang, H. *et al.* The crystal structures of severe acute respiratory syndrome virus main protease and its complex with an inhibitor. *Proc. Natl. Acad. Sci. U. S. A.* **100**, 13190–13195. https://doi.org/10.1073/pnas.1835675100 (2003).
12. Jin, Z. *et al.* Structure of M(pro) from SARS-CoV-2 and discovery of its inhibitors. *Nature* **582**, 289–293. https://doi.org/10.1038/s41586-020-2223-y (2020).
13. Mesecar, A. D. A taxonomically-driven approach to development of potent, broad-spectrum inhibitors of coronavirus main protease including SARS-CoV-2 (COVID-19). http://www.rcsb.org/structure/6W63, https://doi.org/10.2210/pdb6w63/pdb.
14. Su, H. X. *et al.* Identification of a novel inhibitor of SARS-CoV-2 3CLpro. http://www.rcsb.org/structure/6M2N, https://doi.org/10.2210/pdb6m2n/pdb.
15. Zhang, L. *et al.* Crystal structure of SARS-CoV-2 main protease provides a basis for design of improved alpha-ketoamide inhibitors. *Science* https://doi.org/10.1126/science.abb3405 (2020).
16. Xu, Z. *et al.* Nelfinavir was predicted to be a potential inhibitor of 2019-nCov main protease by an integrative approach combining homology modelling, molecular docking and binding free energy calculation. *bioRxiv*, 2020.2001.2027.921627, https://doi.org/10.1101/2020.01.27.921627 (2020).
17. Rut, W. *et al.* Substrate specificity profiling of SARS-CoV-2 main protease enables design of activity-based probes for patient-sample imaging. *bioRxiv*, 2020.2003.2007.981928, https://doi.org/10.1101/2020.03.07.981928 (2020).
18. Chuck, C. P. *et al.* Design, synthesis and crystallographic analysis of nitrile-based broad-spectrum peptidomimetic inhibitors for coronavirus 3C-like proteases. *Eur. J. Med. Chem.* **59**, 1–6. https://doi.org/10.1016/j.ejmech.2012.10.053 (2013).

19. Ghosh, A. K. *et al.* Structure-based design, synthesis, and biological evaluation of peptidomimetic SARS-CoV 3CLpro inhibitors. *Bioorg. Med. Chem. Lett.* **17**, 5876–5880. https://doi.org/10.1016/j.bmcl.2007.08.031 (2007).
20. Ghosh, A. K. *et al.* Design and synthesis of peptidomimetic severe acute respiratory syndrome chymotrypsin-like protease inhibitors. *J. Med. Chem.* **48**, 6767–6771. https://doi.org/10.1021/jm050548m (2005).
21. Goetz, D. H. *et al.* Substrate specificity profiling and identification of a new class of inhibitor for the major protease of the SARS coronavirus. *Biochemistry* **46**, 8744–8752. https://doi.org/10.1021/bi0621415 (2007).
22. Jacobs, J. *et al.* Discovery, synthesis, and structure-based optimization of a series of N-(tert-butyl)-2-(N-arylamido)-2-(pyridin-3-yl) acetamides (ML188) as potent noncovalent small molecule inhibitors of the severe acute respiratory syndrome coronavirus (SARS-CoV) 3CL protease. *J. Med. Chem.* **56**, 534–546. https://doi.org/10.1021/jm301580n (2013).
23. Lee, C. C. *et al.* Structural basis of inhibition specificities of 3C and 3C-like proteases by zinc-coordinating and peptidomimetic compounds. *J. Biol. Chem.* **284**, 7646–7655. https://doi.org/10.1074/jbc.M807947200 (2009).
24. Lee, T. W. *et al.* Crystal structures of the main peptidase from the SARS coronavirus inhibited by a substrate-like aza-peptide epoxide. *J. Mol. Biol.* **353**, 1137–1151. https://doi.org/10.1016/j.jmb.2005.09.004 (2005).
25. Lee, T. W. *et al.* Crystal structures reveal an induced-fit binding of a substrate-like Aza-peptide epoxide to SARS coronavirus main peptidase. *J. Mol. Biol.* **366**, 916–932. https://doi.org/10.1016/j.jmb.2006.11.078 (2007).
26. Lin, D. *et al.* Alpha-ketoamides as broad-spectrum inhibitors of coronavirus and enterovirus replication. http://www.rcsb.org/structure/5N5O, https://doi.org/10.2210/pdb5n5o/pdb.
27. Lu, I. L. *et al.* Structure-based drug design and structural biology study of novel nonpeptide inhibitors of severe acute respiratory syndrome coronavirus main protease. *J. Med. Chem.* **49**, 5154–5161. https://doi.org/10.1021/jm060207o (2006).
28. Shimamoto, Y. *et al.* Fused-ring structure of N-decalin as a novel scaffold for SARS 3CL protease inhibitors. http://www.rcsb.org/structure/5C5N, https://doi.org/10.2210/pdb5c5n/pdb.
29. Shimamoto, Y. *et al.* Fused-ring structure of decahydroisoquinolin as a novel scaffold for SARS 3CL protease inhibitors. *Bioorg. Med. Chem.* **23**, 876–890. https://doi.org/10.1016/j.bmc.2014.12.028 (2015).
30. Turlington, M. *et al.* Discovery of N-(benzo[1,2,3]triazol-1-yl)-N-(benzyl)acetamido)phenyl) carboxamides as severe acute respiratory syndrome coronavirus (SARS-CoV) 3CLpro inhibitors: identification of ML300 and noncovalent nanomolar inhibitors with an induced-fit binding. *Bioorg. Med. Chem. Lett.* **23**, 6172–6177. https://doi.org/10.1016/j.bmcl.2013.08.112 (2013).
31. Yang, H. *et al.* Design of wide-spectrum inhibitors targeting coronavirus main proteases. *PLoS Biol.* **3**, e324. https://doi.org/10.1371/journal.pbio.0030324 (2005).
32. Yang, S. *et al.* Synthesis, crystal structure, structure-activity relationships, and antiviral activity of a potent SARS coronavirus 3CL protease inhibitor. *J. Med. Chem.* **49**, 4971–4980. https://doi.org/10.1021/jm0603926 (2006).
33. Zhang, L., Lin, D. & Hilgenfeld, R. Crystal structure of the complex resulting from the reaction between the SARS-CoV main protease and tert-butyl (1-((S)-3-cyclohexyl-1-(((S)-4-(cyclopropylamino)-3,4-dioxo-1-((S)-2-oxopyrrolidin-3-yl)butan-2-yl)amino)-1-oxopropan-2-yl)-2-oxo-1,2-dihydropyridin-3-yl)carbamate. http://www.rcsb.org/structure/6Y7M, https://doi.org/10.2210/pdb6y7m/pdb.
34. Zhu, L. & Hilgenfeld, R. Crystal structures of SARS-Cov main protease complexed with a series of unsaturated esters. http://www.rcsb.org/structure/3SZN, https://doi.org/10.2210/pdb3szn/pdb.
35. Zhu, L. *et al.* Peptide aldehyde inhibitors challenge the substrate specificity of the SARS-coronavirus main protease. *Antiviral Res.* **92**, 204–212. https://doi.org/10.1016/j.antiviral.2011.08.001 (2011).
36. Jones, G., Willett, P., Glen, R. C., Leach, A. R. & Taylor, R. Development and validation of a genetic algorithm for flexible docking. *J. Mol. Biol.* **267**, 727–748. https://doi.org/10.1006/jmbi.1996.0897 (1997).
37. Friesner, R. A. *et al.* Glide: a new approach for rapid, accurate docking and scoring. 1. Method and assessment of docking accuracy. *J. Med. Chem.* **47**, 1739–1749. https://doi.org/10.1021/jm0306430 (2004).
38. Friesner, R. A. *et al.* Extra precision glide: docking and scoring incorporating a model of hydrophobic enclosure for protein-ligand complexes. *J. Med. Chem.* **49**, 6177–6196. https://doi.org/10.1021/jm051256o (2006).
39. Halgren, T. A. *et al.* Glide: a new approach for rapid, accurate docking and scoring. 2. Enrichment factors in database screening. *J. Med. Chem.* **47**, 1750–1759. https://doi.org/10.1021/jm030644s (2004).
40. London, N. *et al.* Covalent docking of large libraries for the discovery of chemical probes. *Nat. Chem. Biol.* **10**, 1066–1072. https://doi.org/10.1038/nchembio.1666 (2014).
41. Wu, C. Y. *et al.* Stable benzotriazole esters as mechanism-based inactivators of the severe acute respiratory syndrome 3CL protease. *Chem. Biol.* **13**, 261–268. https://doi.org/10.1016/j.chembiol.2005.12.008 (2006).
42. Halgren, T. New method for fast and accurate binding-site identification and analysis. *Chem. Biol. Drug. Des.* **69**, 146–148. https://doi.org/10.1111/j.1747-0285.2007.00483.x (2007).
43. Halgren, T. A. Identifying and characterizing binding sites and assessing druggability. *J. Chem. Inf. Model.* **49**, 377–389. https://doi.org/10.1021/ci800324m (2009).
44. Chaput, L., Martinez-Sanz, J., Saettel, N. & Mouawad, L. Benchmark of four popular virtual screening programs: construction of the active/decoy dataset remains a major determinant of measured performance. *J. Cheminform.* **8**, 56. https://doi.org/10.1186/s13321-016-0167-x (2016).
45. Wishart, D. S. *et al.* DrugBank 5.0: a major update to the DrugBank database for 2018. *Nucleic Acids Res* **46**, D1074–D1082. https://doi.org/10.1093/nar/gkx1037 (2018).
46. Bzowka, M. *et al.* Structural and evolutionary analysis indicate that the SARS-CoV-2 Mpro is a challenging target for small-molecule inhibitor design. *Int. J. Mol. Sci.* https://doi.org/10.3390/ijms21093099 (2020).
47. Krishnamoorthy, N. Variable structural networks at the active site of the SARS-CoV and SARS-CoV2 main proteases. *Preprints* 2020030423, https://doi.org/10.20944/preprints202003.0423.v1 (2020).
48. Goyal, B. & Goyal, D. Targeting the dimerization of the main protease of coronaviruses: a potential broad-spectrum therapeutic strategy. *ACS Comb. Sci.* **22**, 297–305. https://doi.org/10.1021/acscombsci.0c00058 (2020).
49. Choudhary, M. I., Shaikh, M., Tul-Wahab, A. & Ur-Rahman, A. In silico identification of potential inhibitors of key SARS-CoV-2 3CL hydrolase (Mpro) via molecular docking, MMGBSA predictive binding energy calculations, and molecular dynamics simulation. *PLoS ONE* **15**, e0235030. https://doi.org/10.1371/journal.pone.0235030 (2020).
50. Elmezayen, A. D., Al-Obaidi, A., Sahin, A. T. & Yelekci, K. Drug repurposing for coronavirus (COVID-19): in silico screening of known drugs against coronavirus 3CL hydrolase and protease enzymes. *J. Biomol. Struct. Dyn.* https://doi.org/10.1080/07391102.2020.1758791 (2020).
51. Hage-Melim, L. *et al.* Virtual screening, ADME/Tox predictions and the drug repurposing concept for future use of old drugs against the COVID-19. *Life Sci.* **256**, 117963. https://doi.org/10.1016/j.lfs.2020.117963 (2020).
52. Mittal, L., Kumari, A., Srivastava, M., Singh, M. & Asthana, S. Identification of potential molecules against COVID-19 main protease through structure-guided virtual screening approach. *J. Biomol. Struct. Dyn.* https://doi.org/10.1080/07391102.2020.1768151 (2020).
53. Wu, C. *et al.* Analysis of therapeutic targets for SARS-CoV-2 and discovery of potential drugs by computational methods. *Acta Pharm. Sin. B* https://doi.org/10.1016/j.apsb.2020.02.008 (2020).
54. Tralau-Stewart, C. J. *et al.* GSK256066, an exceptionally high-affinity and selective inhibitor of phosphodiesterase 4 suitable for administration by inhalation: in vitro, kinetic, and in vivo characterization. *J. Pharmacol. Exp. Ther.* **337**, 145–154. https://doi.org/10.1124/jpet.110.173690 (2011).

55. Harder, E. *et al.* OPLS3: a force field providing broad coverage of drug-like small molecules and proteins. *J. Chem. Theory Comput* **12**, 281–296. https://doi.org/10.1021/acs.jctc.5b00864 (2016).
56. Achdout, H. *et al.* COVID Moonshot: open science discovery of SARS-CoV-2 main protease inhibitors by combining crowdsourcing, high-throughput experiments, computational simulations, and machine learning. *bioRxiv*, 2020.2010.2029.339317, https://doi.org/10.1101/2020.10.29.339317 (2020).

Acknowledgements
We thank Craig Coel and Katalin Phimister from Schrödinger for all their support, Haim Barr and Nir London for their help and all Kobiler lab members for their comments.

Author contributions
A.S. and O.Ko. designed research; A.S., D.Z., O.Ka., I.B., D.D., T.Y., I.B., I.S., E.B.Z. and E.S. analyzed data; A.S., D.Z., O.Ka., I.B., D.D., T.Y., I.B., I.S., E.B.Z. and E.S. performed research; A.S. and O.Ko. wrote the paper.

Funding
This work was supported by grants from the Israel Science foundation (Grant #1387/14) to O.K. The funders had no role in study design, data collection and analysis, decision to publish, or preparation of the manuscript.

Competing interests
The authors declare no competing interests.

Additional information
Supplementary information is available for this paper at https://doi.org/10.1038/s41598-020-77794-5.

Correspondence and requests for materials should be addressed to O.K.

Reprints and permissions information is available at www.nature.com/reprints.

Publisher's note Springer Nature remains neutral with regard to jurisdictional claims in published maps and institutional affiliations.